Inorganic Chemistry

ARTICLE

pubs.acs.org/IC

# Fast Carbon Dioxide Fixation by 2,6-Pyridinedicarboxamidato-nickel(II)-hydroxide Complexes: Influence of Changes in Reactive Site Environment on Reaction Rates

Deguang Huang,[†] Olga V. Makhlynets,[‡] Lay Ling Tan,[§] Sonny C. Lee,[*,§] Elena V. Rybak-Akimova,[*,‡] and R. H. Holm[*,†]

[†]Department of Chemistry and Chemical Biology, Harvard University, Cambridge, Massachusetts 02138, United States

[‡]Department of Chemistry, Tufts University, Medford, Massachusetts 02155, United States

[§]Department of Chemistry, University of Waterloo, Waterloo, Ontario N2L3G1, Canada

*Supporting Information*

**ABSTRACT:** The planar complexes $[\mathrm{Ni^{II}(pyN_2^{R2})(OH)}]^-$, containing a terminal hydroxo group, are readily prepared from *N,N*′-(2,6-$C_6H_3R_2$)-2,6-pyridinedicarboxamidate(2-) tridentate pincer ligands $(R_4N)(OH)$, and $Ni(OTf)_2$. These complexes react cleanly and completely with carbon dioxide in DMF solution in a process of $CO_2$ fixation with formation of the bicarbonate product complexes $[\mathrm{Ni^{II}(pyN_2^{R2})(HCO_3)}]^-$ having $\eta^1$-$OCO_2H$ ligation. Fixation reactions follow second-order kinetics (rate = $k_2'[\mathrm{Ni^{II}{-}OH}][\mathrm{CO_2}]$) with negative activation entropies (−17 to −28 eu). Reactions were monitored by growth and decay of metal-to-ligand charge-transfer (MLCT) bands at 350−450 nm. The rate order R = Me > macro > Et > Pr$^i$ > Bu$^i$ > Ph at 298 K (macro = macrocylic pincer ligand) reflects increasing steric hindrance at the reactive site. The inherent highly reactive nature of these complexes follows from $k_2' \approx 10^6\ \mathrm{M^{-1}\ s^{-1}}$ for the R = Me system that is attenuated by only 100-fold in the R = Ph complex. A reaction mechanism is proposed based on computation of the enthalpic reaction profile for the R = Pr$^i$ system by DFT methods. The R = Et, Pr$^i$, and Bu$^i$ systems display biphasic kinetics in which the initial fast process is followed by a slower first order process currently of uncertain origin.

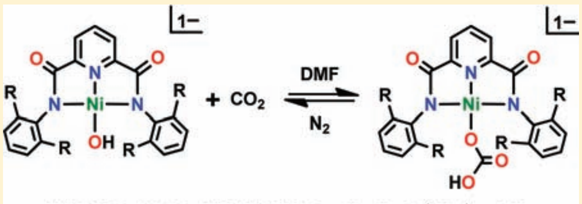

KINETICS OF $CO_2$ FIXATIONS: R = Me, Et, Pr$^i$, Bu$^i$ and Ph

## INTRODUCTION

In the present context, carbon dioxide fixation is a recognized reaction type by which $CO_2$ is converted to bicarbonate or carbonate by reaction with metal-bound hydroxo groups. With trivalent metals, the reactions frequently employ terminal $M^{III}$−OH groups of chromium and cobalt and afford $\eta^1$-bicarbonate species as the initial product.[1−4] With divalent metals, the reactions proceed with terminal or bridging hydroxo ligation and yield products that often contain carbonate bound in binuclear or trinuclear bridging modes. Numerous examples of these reactions are found with complexes of $Co^{II}$, $Ni^{II}$, $Cu^{II}$, and $Zn^{II}$ in particular.[5−14] In the case of $Ni^{II}$, nearly all reactions utilize bridged Ni-$(OH)_{1,2}$-Ni units and lead to products in which carbonate is stabilized by $\eta^2$- or $\eta^3$-coordination to two $Ni^{II}$ atoms.[5,15−18]

In contrast to foregoing reactions, we have discovered reaction 1 in Figure 1, which has several notable features.[19] The reactant contains an infrequent example of the terminal $Ni^{II}$−OH group,[20−24] apparently stabilized by the steric protection provided by the 2,6-dimethylphenyl substituents of the tridentate 2,6-pyridinedicarboxamidate pincer ligand. Although comparisons are inexact owing to differences in solvent, the second-order rate constant $k_2 = 9.5 \times 10^5\ \mathrm{M^{-1}\ s^{-1}}$ in DMF at 298 K[19] is the highest reported value for nonenzymatic carbon dioxide fixation and overlaps with the lower end of estimated rate constants for human carbonic anhydrase in aqueous solution ($k_2 = k_{cat}/K_M \sim 10^6 - 10^8\ \mathrm{M^{-1}\ s^{-1}}$).[10] The enthalpic profile of this reaction computed by density functional theory (DFT) methods provides useful insight into the stationary point structures along the reaction pathway. In this investigation, we have sought additional characterization of this mode of carbon dioxide fixation. The influence of changes in environment at the $Ni^{II}$−OH reactive group has been examined by determining the kinetics of five additional systems based on the $pyN_2^{R2}$ ligand platform. In addition, we have found in several fixation reaction systems a second measurable kinetics process.

## EXPERIMENTAL SECTION

**Preparation of Compounds.** All reactions and manipulations in the preparation of $Ni^{II}$ compounds were performed under a dinitrogen atmosphere using either Schlenk techniques or an inert atmosphere box. Volume reduction and drying steps were performed in vacuo.

**Received:** May 5, 2011
**Published:** September 09, 2011

ACS Publications © 2011 American Chemical Society

dx.doi.org/10.1021/ic200942u | *Inorg. Chem.* 2011, 50, 10070–10081

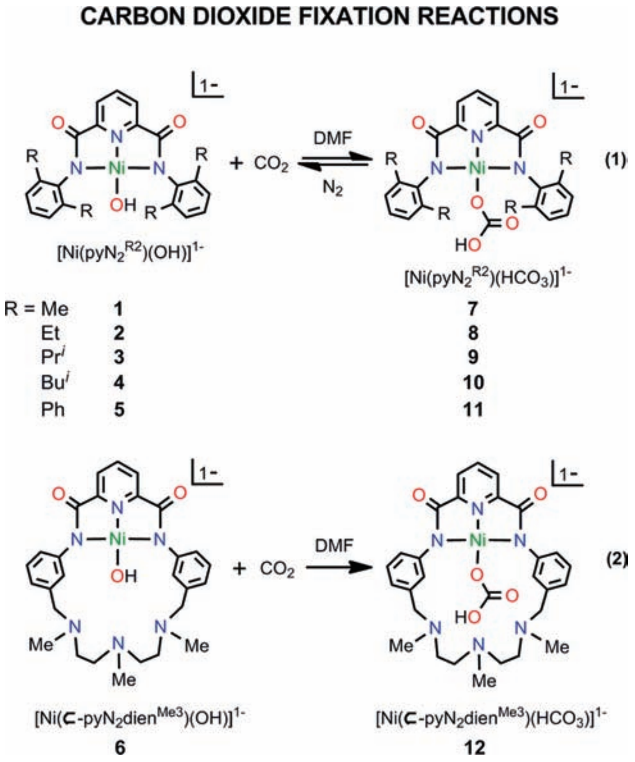

**Figure 1.** Depiction of $CO_2$ fixation reactions of *N*,*N*′-disubstituted 2,6-pyridinedicarboxamidato-$Ni^{II}$−OH complexes and a macrocyclic complex containing the same pincer chelate group. Numerical designations of initial hydroxo and product bicarbonato complexes are indicated.

Commercial grade chemicals were used without further purification. Tetrahydrofuran (THF) and diethyl ether were purified by an Innovative Technology or MBraun purification system. Dimethylformamide (DMF) was freshly distilled from $CaH_2$ in vacuo at 55 °C and purged with dinitrogen gas. All solvents were degassed before use. Compounds were identified by a combination of spectroscopic and crystallographic methods; representative compounds were analyzed (Midwest Microlab). Cation resonances are omitted from $^1$H NMR data. The compounds $H_2pyN_2^{Me2}$, $(Et_4N)[Ni(pyN_2^{Me2})(OH)]$, $(Et_4N)[Ni(pyN_2^{Me2})(HCO_3)]$, $(Et_4N)[Ni(\subset\text{-}pyN_2dien^{Me3})(OH)]$, and $(Et_4N)[Ni(\subset\text{-}pyN_2dien^{Me3})(HCO_3)]$ were prepared as described.[25,26]

**Pincer Ligands: *N*,*N*′-disubstituted 2,6-Pyridinedicarboxamidates, $H_2pyN_2^{R2}$.** The procedure for the **R** = **Et** ligand is typical. To a mixture of 2,6-diethylaniline (1.49 g, 10.0 mmol) and triethylamine (1.67 mL, 12.0 mmol) in THF (150 mL) at 0 °C was added slowly a solution of pyridine-2,6-dicarbonylchloride (1.22 g, 6.00 mmol). The reaction mixture was warmed to room temperature, stirred for 15 h, and filtered. Solvent was removed and the light yellow mixture was purified on a silica column eluted with dichloromethane/methanol/$NH_4OH$ (150/5/1 v/v/v). The colorless oily residue after solvent removal was treated with hexane (10 mL) and dried to give the pure product as a white powder (1.97 g, 92%). $^1$H NMR ($CDCl_3$): $\delta$ 1.21 (t, 12), 2.66 (q, 8), 7.19 (d, 4), 7.28 (m, 2), 8.17 (t, 1), 8.55 (d, 2), 9.08 (s, 2). **R** = **Pr$^i$**: 10 mmol scale, 2.27 g, 94%. $^1$H NMR ($CDCl_3$): $\delta$ 1.23 (d, 24), 3.15 (m, 4), 7.24 (d, 4), 7.36 (t, 2), 8.19 (t, 1), 8.56 (d, 2), 9.01 (s, 2). **R** = **Bu$^i$**: 2.4 mmol scale, 0.57 g, 88%. $^1$H NMR ($CDCl_3$): $\delta$ 0.84 (d, 24), 1.84 (m, 4), 2.49 (d, 8), 7.13 (d, 4), 7.23 (t, 2), 8.16 (t, 1), 8.57 (d, 2), 9.08 (s, 2). ***N*,*N*′-bis(1-naphthyl)-2,6-pyridinedicarboximidate:** 5.0 mmol scale, solvent acetonitrile (no chromatography step), 1.63 g, 78%. $^1$H NMR ($(CD_3)_2SO$): $\delta$ 7.70 (d, 2), 7.91 (d, 2), 7.99 (d, 2), 8.10 (d, 2), 8.35 (t, 1), 8.45 (d, 2), 11.44 (s, 2). ***N*,*N*′-bis(1-adamantyl)-2,6-pyridinedicarboximidate:** 10 mmol scale, 1.62 g, 75%. $^1$H NMR ($CDCl_3$): $\delta$ 1.74 (s, 18), 2.15 (s, 12), 7.48 (s, 2), 7.80 (t, 1), 8.27 (d, 2).

**$H_2pyN_2^{Ph2}$.** An adaptation of a previous procedure[27] was used for the synthesis of precursor 2,6-diphenylaniline. Under anaerobic conditions a solution of $PhB(OH)_2$ (2.19 g, 18.0 mmol) in ethanol (12 mL) was added to a solution of 2,6-dibromoaniline (1.51 g, 6.00 mmol) in toluene (60 mL). Aqueous $Na_2CO_3$ solution (2 M, 25 mL) and $Pd(PPh_3)_4$ (0.83 g, 0.72 mmol) were added, and the mixture was refluxed for 20 h at 85 °C. The organic layer was separated, and the aqueous phase extracted with ether (3 × 50 mL). The combined organic phases were dried over $MgSO_4$ in air, and solvent was removed. The black residue was purified on a silica column eluted with ethyl acetate/petroleum ether (1/9 v/v). Solvent was removed from the eluate, and the residue was crystallized from hot hexanes to afford pure 2,6-diphenylaniline as a white solid (1.25 g, 85%). $^1$H NMR ($CDCl_3$): $\delta$ 3.87 (br, 2), 6.93 (t, 1), 7.17 (d, 2), 7.39 (t, 2), 7.49 (t, 4), 7.55 (d, 4). A solution of pyridine-2,6-dicarbonylchloride (0.61 g, 3.00 mmol) was added slowly to a mixture of 2,6-diphenylaniline (1.25 g, 5.10 mmol) and triethylamine (0.83 mL, 6.00 mmol) in THF (120 mL) at 0 °C. The mixture was stirred for 40 h and filtered. Solvent was removed, and the residue was purified on a silica column eluted with dichloromethane and dichloromethane/methanol/$NH_4OH$ (150:10:1 v/v/v) in succession to give the pure product as a white solid (1.27 g, 80%). $^1$H NMR ($CDCl_3$): $\delta$ 7.26 (t, 4), 7.34 (t, 8), 7.45 (d, 8), 7.51 (m, 6), 7.78 (t, 1), 7.97 (d, 2), 8.58 (s, 2).

**$(Et_4N)[Ni(pyN_2^{Et2})(OH)]$.** $H_2pyN_2^{Et2}$ (86 mg, 0.20 mmol) and $Ni(OTf)_2$ (71 mg, 0.20 mmol) were stirred in DMF (3 mL) for 1 h. The light yellow suspension was treated with $Et_4NOH$ (25% in methanol, 176 mg, 0.30 mmol) and stirred for 1 h to give a red suspension. A second equal portion of $Et_4NOH$ was added, and the mixture was stirred for 10 h to form a deep red solution. The mixture was filtered through Celite and ether (20 mL) was added to the filtrate to deposit a red oil which was taken up in THF (3 mL) and treated with ether (10 mL) to afford a red solid. This material was washed with ether, THF, and ether and dried to give the product as a red crystalline solid (78 mg, 62%). Absorption spectrum (DMF): $\lambda_{max}$ ($\varepsilon_M$) 413 (5200), 486 (sh, 2300) nm; ($CH_2Cl_2$): $\lambda_{max}$ ($\varepsilon_M$) 407 (5180), 477 (sh, 2200) nm. $^1$H NMR (DMF-$d_7$): $\delta$ −5.08 (s, 1), 1.34 (t, 12), 2.98 (q, 8), 6.88 (s, br, 6), 7.52 (d, 2), 8.07 (t, 1). *Anal.* Calcd. for $C_{35}H_{50}N_4NiO_3$: C, 66.36; H, 7.96; N, 8.84. Found: C, 66.44; H, 8.00; N, 8.86.

**$(Et_4N)[Ni(pyN_2^{iPr2})(OH)]$.** The preceding method was employed on the same scale with use of $H_2pyN_2^{iPr2}$. The red oil was treated with ether (5 mL) to form an orange-red solid, which was dissolved in a minimal volume of THF. The solution was stored at −20 °C overnight, filtered, and ether added to the filtrate. The red material deposited was washed with ethyl acetate (4 × 5 mL) and ether, and dried to afford the product as a red solid (69 mg, 50%). Absorption spectrum (DMF): $\lambda_{max}$ ($\varepsilon_M$) 413 (4580), 486 (sh, 2070) nm. $^1$H NMR (THF-$d_8$): $\delta$ −5.25 (s, 1), 1.15 (d, 12), 1.38 (d, 12), 4.01 (m, 4), 6.89 (s, 6), 7.44 (d, 2), 7.86 (t, 1). *Anal.* Calcd. for $C_{39}H_{58}N_4NiO_3$: C, 67.93; H, 8.48; N, 8.12. Found: C, 67.85; H, 8.55; N, 8.03.

**$(Me_4N)[Ni(pyN_2^{iBu2})(OH)]$.** The preceding method was used on a 0.10 mmol scale with use of $H_2pyN_2^{iBu2}$ and $Me_4NOH$ (25% in methanol). After the addition of the second portion of this reagent, the mixture was stirred for 15 h, filtered through Celite, and ether (20 mL) was added. The mixture was filtered and addition of a second portion of ether (30 mL) resulted in precipitation of a red oily material that was washed with THF (4 mL) and dissolved in THF/DMF (1 mL, 7:3 v/v). Ethyl acetate was added slowly to precipitate a colorless solid. The mixture was filtered, and ether was added to the filtrate to form a red solid, which was washed with THF (4 mL) and dissolved in toluene/DMF (2 mL, 10:1 v/v). Ether was diffused into this solution to give the product as a red crystalline solid (26 mg, 38%). Absorption spectrum (DMF): $\lambda_{max}$ ($\varepsilon_M$) 414 (4700), 486 (sh, 2100) nm. $^1$H NMR

(DMF-$d_7$): $\delta$ −5.15 (s, 1), 0.94 (m, 24), 2.55 (m, 4), 2.65 (m, 4), 3.15 (m, 4), 6.82 (s, 6), 7.49 (d, 2), 8.03 (t, 1).

**$(Me_4N)[Ni(pyN_2^{Ph2})(OH)]$.** $H_2pyN_2^{Ph2}$ (62 mg, 0.10 mmol) and $Ni(OTf)_2$ (36 mg, 0.10 mmol) were stirred in DMF for 1 h. The light yellow mixture was treated with $Me_4NOH$ (25% in methanol, 55 mg, 0.15 mmol) and stirred for 1 h to give a red suspension. A second equal portion of $Me_4NOH$ was added, and the mixture was stirred for 5 h to afford a dark red solution, which was filtered through Celite. Ether (15 mL) was added to the filtrate to deposit an orange-red solid. The solid was stirred in THF/propionitrile (8 mL, 3:1 v/v) for 45 min and filtered through Celite to remove a sticky precipitate. Ether was added to the filtrate to deposit a red solid that was taken up in THF/DMF (3.5 mL, 6:1 v/v) to form a saturated solution. Toluene (3 mL) was slowly added; after 1 h the solution was filtered to remove a colorless solid. The red filtrate was diffused with ether to deposit the product as block-like red crystals (23 mg, 30%) together with a small amount of colorless crystals which were separated manually. Absorption spectrum (DMF): $\lambda_{max}$ ($\varepsilon_M$) 414 (4050), 486 (sh, 1800) nm. $^1$H NMR (DMF-$d_7$): $\delta$ −4.86 (s, 1), 7.02 (d, 2), 7.10 (d, 4), 7.16 (t, 2), 7.31 (m, 12), 7.64 (t, 1), 8.05 (m, 8).

**$(Et_4N)[Ni(pyN_2^{Et2})(HCO_3)]$.** A solution of $(Et_4N)[Ni(pyN_2^{Et2})(OH)]$ (25 mg, 0.040 mmol) in DMF (2 mL) was bubbled with carbon dioxide for 20 min. Diffusion of ether saturated with carbon dioxide into the red solution resulted in separation of the product as block-like red crystals (22 mg, 81%). Absorption spectrum (DMF): $\lambda_{max}$ ($\varepsilon_M$) 306 (7250), 378 (5600), 477 (sh, 940) nm; ($CH_2Cl_2$): $\lambda_{max}$ ($\varepsilon_M$) 304 (7070), 379 (5600), 477 (sh, 990) nm. $^1$H NMR (DMF-$d_7$): $\delta$ 1.28 (m, 12), 3.13 (m, br, 8), 6.84 (s, 6), 7.55 (s, 2), 8.16 (t, 1).

### Chart 1. Abbreviations and Designation of Complexes

| | |
|---|---|
| $[Ni(pyN_2^{R2})(OH)]^{1-}$ | R = Me[19,25] **1**, Et **2**, Pr$^i$ **3**<br>Bu$^i$ **4**, Ph **5** |
| $[Ni(\subset\text{-}pyN_2dien^{Me3})(OH)]^{1}$ | **6**[25] |
| $[Ni(pyN_2^{R2})(HCO_3)]^{1-}$ | R = Me[19,25] **7**, Et **8**, Pr$^i$ **9**<br>Bu$^i$ **10**, Ph **11** |
| $[Ni(\subset\text{-}pyN_2dien^{Me3})(HCO_3)]^{1-}$ | **12**[25] |

DIPP = diisopropylphenyl, DMP = dimethylphenyl, nap = 1-naphthyl, $pyN_2^{R2}$ = *N*,*N'*-bis(2,6-$R_2$-phenyl)-2,6-pyridinedicarboxamidate(2-), $\subset$-$pyN_2dien^{Me3}$ = bis(phenyl-3,3'-(2,5,8-tri-*N*-methylamino-1,9-nonyl)-2,6-pyridinedicarboxamidate(2-), TfO = triflate(1-)

In the sections that follow, complexes are numerically designated as in the Chart 1.

**X-ray Structure Determinations.** The structures of the seven compounds in Tables 1 and 2 were determined; for brevity, compounds are referred to by their anion number. Diffraction-quality crystals were obtained from the following solvents: DMF/ether (**2**, **8**, **9**, **12**), DMF/ethyl acetate (**3**), DMF/toluene/ether (**4**, **5**). Diffraction data were collected on a Bruker CCD area detector diffractometer equipped with an Oxford 700 low-temperature apparatus. Structures were solved by direct methods using the SHELX program package.[28] The ether solvate molecule in **4** was treated as disordered with two equally occupied

### Table 2. Crystallographic Data for Compounds Containing $[Ni(pyN_2^{R2})(HCO_3)]^{-a}$

| compounds | $(Et_4N)$[**8**] | $(Et_4N)$[**9**] | $(Et_4N)$[**12**] |
|---|---|---|---|
| formula | $C_{36}H_{50}N_4NiO_5$ | $C_{40}H_{58}N_4NiO_5$ | $C_{37}H_{53}N_7NiO_5$ |
| *M* | 677.51 | 733.61 | 734.57 |
| crystal system | monoclinic | orthorhombic | triclinic |
| space group | $P2_1/n$ | *Pnma* | $P\bar{1}$ |
| *a*, Å | 15.172(2) | 22.679(2) | 10.521(5) |
| *b*, Å | 12.394(1) | 11.6237(8) | 13.400(6) |
| *c*, Å | 19.098(2) | 14.917(1) | 15.030(7) |
| $\alpha$, deg | 90 | 90 | 95.953(9) |
| $\beta$, deg | 102.029(2) | 90 | 104.788(9) |
| $\gamma$, deg | 90 | 90 | 112.368(8) |
| *V*, Å$^3$ | 3512.5(6) | 3932.3(5) | 1846.1(15) |
| *Z* | 4 | 4 | 2 |
| $\mu$, mm$^{-1}$ | 0.599 | 0.540 | 0.577 |
| independent data | 6427 | 4217 | 6626 |
| refined parameters | 768 | 338 | 605 |
| $R_1{}^b$, $wR_2{}^c$ ($I > 2\sigma(I)$) | 0.0807, 0.2312 | 0.0798, 0.2290 | 0.0615, 0.1629 |
| $R_1$, $wR_2$ (all data) | 0.1039, 0.2666 | 0.0951, 0.2498 | 0.0955, 0.1884 |

[a] $T = 100(2)$ K, Mo K$\alpha$ radiation ($\lambda = 0.71073$ Å). [b] $R_1 = \Sigma||F_o| - |F_c||/\Sigma|F_o|$. [c] $wR_2 = \{\Sigma[w(F_o^2 - F_c^2)^2/(F_o^2)^2]\}^{1/2}$.

### Table 1. Crystallographic Data for Compounds Containing $[Ni(pyN_2^{R2})(OH)]^{-a}$

| | $(Et_4N)$[**2**] | $(Et_4N)$[**3**]$\cdot MeCO_2Et$ | $(Me_4N)$[**4**]$\cdot Et_2O$ | $\{(Me_4N)$[**5**]$\}_5\cdot$3DMF |
|---|---|---|---|---|
| formula | $C_{35}H_{50}N_4NiO_3$ | $C_{43}H_{66}N_4NiO_5$ | $C_{43}H_{68}N_4NiO_4$ | $C_{244}H_{231}N_{23}Ni_5O_{18}$ |
| *M* | 633.50 | 777.71 | 763.72 | 2967.3 |
| crystal system | orthorhombic | monoclinic | orthorhombic | monoclinic |
| space group | $Pca2_1$ | $P2_1/c$ | $P2_12_12_1$ | $P2_1/n$ |
| *a*, Å | 16.1746(6) | 14.817(2) | 15.7551(6) | 18.031(1) |
| *b*, Å | 25.954(1) | 14.424(2) | 16.2340(6) | 50.315(3) |
| *c*, Å | 15.7902(6) | 19.689(2) | 17.6627(7) | 23.340(2) |
| $\alpha$, deg | 90 | 90 | 90 | 90 |
| $\beta$, deg | 90 | 93.352(2) | 90 | 98.914(1) |
| $\gamma$, deg | 90 | 90 | 90 | 90 |
| *V*, Å$^3$ | 6628.8(4) | 4200.6(7) | 4517.6(3) | 20919(2) |
| *Z* | 8 | 4 | 4 | 4 |
| $\mu$, mm$^{-1}$ | 0.625 | 0.509 | 0.471 | 0.513 |
| independent data | 12593 | 10422 | 8565 | 39803 |
| refined parameters | 776 | 497 | 493 | 2616 |
| $R_1{}^b$, $wR_2{}^c$ ($I > 2\sigma(I)$) | 0.0360, 0.0847 | 0.0428, 0.1077 | 0.0688, 0.1922 | 0.0532, 0.1109 |
| $R_1$, $wR_2$ (all data) | 0.0400, 0.0877 | 0.0590, 0.1185 | 0.0837, 0.2083 | 0.0752, 0.1201 |

[a] $T = 100(2)$ K, Mo K$\alpha$ radiation ($\lambda = 0.71073$ Å). [b] $R_1 = \Sigma||F_o| - |F_c||/\Sigma|F_o|$. [c] $wR_2 = \{\Sigma[w(F_o^2 - F_c^2)^2/(F_o^2)^2]\}^{1/2}$.

positions and atoms were described isotropically. The unit cell of **5** presents a very long *b*-axis owing to an unusual independent unit in the structure; the cell contains four crystallographically independent units, each of which has five anions, five cations, and three DMF solvate molecules. All atoms in **8** were disordered in two positions with 3:2 occupancies in the cation and 1:1 in the cation, except for two carbon atoms of one ethyl group which was treated as disordered over three positions with occupancies of 4:3:3. Structure **9** has a crystallographic mirror plane containing $NiN_3$. The two independent isopropyl groups were disordered over two positions with 85/15 and 60/40 occupancies; carbon atoms of two ethyl groups of the cation also showed a 60/40 disorder. The two phenyl rings and the dien chain of **12** are disordered in two positions with 55/45 occupancies. Hydrogen atoms were not added to cations or solvate molecules in **4** and **9** owing to disordered carbon atoms. The hydrogen atoms of the −OH groups of **2**−**5** were located geometrically. However, the hydrogen atom of the -$HCO_3$ group of **12** was located from difference Fourier maps and refined isotropically. The hydrogen atom was not added to the -$HCO_3$ group of **8** because of its highly disordered oxygen atoms. Crystal data and refinement details are given in Tables 1 and 2.[29] The compound tetraethylammonium [*N*,*N*′-bis(1-naphthyl)-2,6-pyridinedicarboximidato]$Ni^{II}$ crystallizes in monoclinic space group $P2_1/c$ with $a = 30.170(7)$ Å, $b = 24.581(6)$ Å, $c = 19.054(4)$ Å, $\beta = 104.251(4)°$, $V = 13.696(5)$ Å$^3$; the structure was refined to $R_1$ ($wR_2$) = 0.0959 (0.1491) (all data).[29] Other refinement details and explanations (wherever necessary) are included in individual CIF files.

**Kinetics Measurements.** Kinetics of the reactions between $Ni^{II}$ complexes **2**−**6** and carbon dioxide were determined in DMF solutions. Commercial DMF was dried over 3 Å molecular sieves for 3 d and then distilled from $CaH_2$ under vacuum (55 °C) and degassed by purging with dry dinitrogen before use in an MBraun inert atmosphere box filled with argon. Solutions of each complex were prepared immediately before a kinetics run and were placed in Hamilton gastight syringes equipped with three-way valves. Saturated solutions of $CO_2$ in DMF (0.20 M[30,31]) were prepared by bubbling $CO_2$ gas through argon-saturated DMF in a syringe at 298 K for 20 min. Solutions of lower concentrations of $CO_2$ were prepared by serial dilution of the 0.20 M solution with argon-saturated DMF using graduated gastight syringes; liquid phase occupied the entire available volume in the closed system and was never exposed to the atmosphere and/or the gas/vapor phase. Kinetics measurements were performed on a TgK Scientific (formerly HiTech Scientific, Salisbury, Wiltshire, U.K.) SF-61DX2 cryogenic stopped-flow system (mixing time 2−4 ms) equipped with tungsten and xenon arc lamps. Solutions of the $Ni^{II}$ complexes and $CO_2$ in DMF were separately thermostatted at low temperature (218−283 K) and mixed in a 1:1 volume ratio. The mixing cell temperature was maintained at ±0.1 K. Concentrations of all reagents are reported for the onset of the reaction (after mixing). $CO_2$ (0.4−10 mM) was always in excess to the $Ni^{II}$ complex (usually 0.1 mM). Because the reactions are fast, data were collected in a single-wavelength mode; repeated scans over a range of wavelengths allowed reconstruction of time-resolved spectra. For each complex, a series of kinetics traces in the range 370−450 nm were collected in steps of 3−5 nm. In this way, the two processes were separated and rate constants determined for each.

All complexes showed the formation and decay of an intermediate at 380−390 nm. The spectroscopic contributions of the second process were negligible for **6** where essentially single-exponent behavior over the entire spectral range was observed. Similarly, for **1** absorbance changes due to the second process were very small at 370−390 nm, and the complex displayed single-exponent kinetics when the reaction was monitored at 400−500 nm.[19] Rate constants were determined with Kinetic Studio (TgK Scientific) and IgorPro programs using single-exponential (A→B) or double-exponential (A→B→C) models. Kinetics parameters for single-step processes were determined from single-exponential fits to the pseudo-first-order rate law $A = A_\infty + \Delta A \exp(-kt)$ where $A_\infty$ is the absorbance of the reaction mixture after the reaction is complete and $\Delta A = A_0 - A_\infty$ where $A_0$ is the initial absorbance. Similarly, double-exponential kinetics were analyzed using $A = A_\infty + \Delta A_1 \exp(-k_1 t) + \Delta A_2 \exp(-k_2 t)$ in which $\Delta A_{1,2}$ and $k_{1,2}$ were used as fitting parameters. Each reported rate constant is an average of at least 7 runs with a standard deviation within 2%. To evaluate activation parameters for each complex, variable temperature measurements were performed at a wavelength that showed most clearly the growth of the intermediate followed by its decay; linear Eyring plots ($k_2' = [(k_B T/h) \exp(-\Delta G^\ddagger/RT)$ with $\Delta G^\ddagger = \Delta H^\ddagger - T\Delta S^\ddagger$) were obtained for the fast (direct reaction with $CO_2$) and slow processes of several complexes (**2**, **3**, **4**) and for the fast process of the remaining complexes (**5**, **6**) which did not exhibit sufficient absorbance changes for evaluation of the slow process.

**Computational Methods.** Density functional calculations were performed using the Gaussian 09 software package.[32] Stationary points and associated transition energies were characterized using the BP86 functional[33,34] and 6-31G(d) basis set[35,36] following our previously reported protocol.[19] For time-dependent DFT (TD-DFT) calculations,[37] the 200 lowest energy singlet transitions, fully spanning the 250−650 nm range, were determined using the B3LYP functional[33,38,39] and 6-31G(d) basis set;[35,36] additional test calculations investigated the effects of other functional (BP86) and basis set (6-31+G(d),[40] LanL2DZ[41]) combinations and solvation (polarizable continuum model).[42] Electronic spectra were simulated with transitions represented by Gaussian functions with full-width at half-maximum values of 3000 cm$^{-1}$ (GaussSum 2.2).[43] Different functionals (BP86, B3LYP) and basis sets (LanL2DZ, 6-31G(d), 6-31+G(d)), in the gas phase and with a continuum solvent model (PCM, DMF solvent), were investigated, and the simulated spectra compared against the experimental spectra of selected hydroxo and bicarbonate complexes. Empirically, B3LYP calculations were significantly better at reproducing the general features in the experimental spectra. Gas phase B3LYP/6-31G(d) calculations yielded the best quantitative results in terms of band maxima and intensities at reasonable computational cost. Qualitative assignments for the electronic transitions were obtained by visual inspection of orbital surfaces (GaussView)[44] and Mulliken population analysis[45] of relevant fragment orbital contributions (QMForge).[46]

## ■ RESULTS AND DISCUSSION

A DFT analysis of the enthalpic profile of reaction 1 in which hydroxo complex **1** is converted to bicarbonate product **7** indicates a low activation enthalpy and attendant unusually high reaction rate. We interpret this property to originate in major part from the favorable steric accessibility of the small substrate to the $Ni^{II}$−OH functional group. In addition, there are minimal structural changes of the complex in the fixation process.[19] To better understand this reaction type, it is significant to identify factors that increase or decrease the reaction rate in a constant medium while maintaining the essential NNN pincer ligand platform.

**Reactant Complexes Containing the $Ni^{II}$−OH Group.** The most accessible molecular structural variables are the N-substituents, the decreased size of which compared to 2,6-dimethylphenyl in **1** might be expected to increase rates because of enhanced access to the reactive site. However, phenyl[47] or other groups of about the same size or smaller[48−50] stabilize octahedral bis-ligand complexes instead of the desired planar stereochemistry. Also, a 1:1 reaction of the *N*,*N*′-bis(1-naphthyl) ligand and $Ni(OTf)_2$ gave octahedral [*N*,*N*′-bis(1-naphthyl)-2,6-pyridinedicarboximidato]$Ni^{II}$, identified crystallographically.[29] In an attempt to obtain a 1:1 complex with an aliphatic substituent, the *N*,*N*′-bis(1-adamantyl) ligand was prepared, but it did not form a $Ni^{II}$ complex. Ligands with

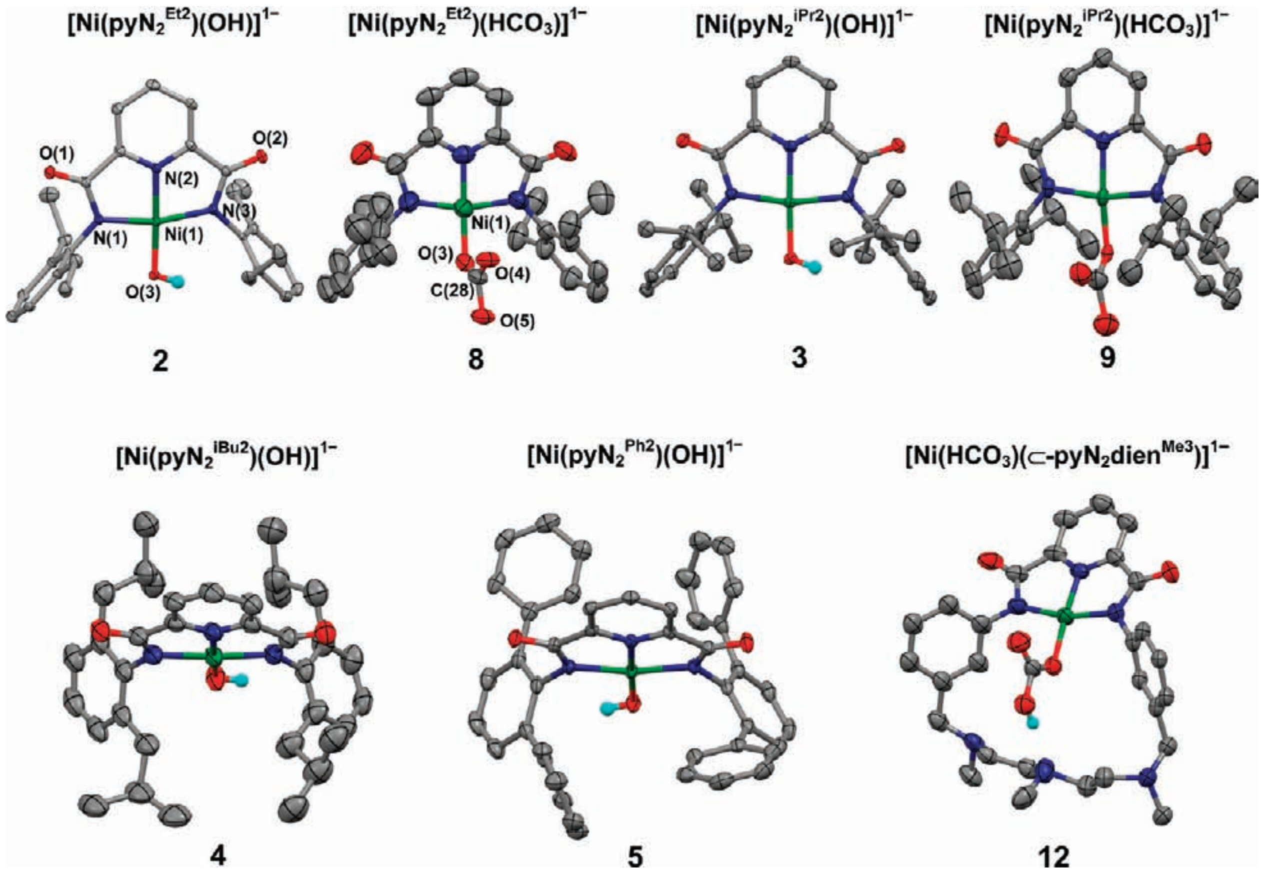

**Figure 2.** Structures of the complexes $[Ni^{II}(pyN_2^{R2})(OH)]^-$ with R = Et (**2**), Pr$^i$ (**3**), Bu$^i$ (**4**), Ph (**5**), and $[Ni^{II}(pyN_2^{R2})(HCO_3)]^-$ with R = Et (**8**), Pr$^i$ (**9**), and macro (**12**) showing 50% probability ellipsoids. Bond distances (Å) and angles (deg) in the hydroxo series are nearly invariant and are represented by **2:** Ni−N1 1.924(2), Ni−N2 1.825(2), Ni−N3 1.917(2), Ni−O3 1.828(2), N1−Ni−N2 82.7(1), N2−Ni−N3 82.4(1), N1−Ni−O3 96.0(1), N3−Ni−O3 98.9(1), N2−Ni−O3 177.6(1), N1−Ni−N3 165.1(1). For other complexes, Ni−O3 = 1.820(2) (**3**), 1.822(3) (**4**), 1.835(9) (**5**). The structures of **8**, **9**, and **12** in the Ni−N3 region are very similar to those of **2**. For **8**: Ni−O3 1.87(1), Ni−O3−C28 = O4−C28−O5 117(2), O3−C28−O4 128(2), O4−C28−O5 117(2).

2,6-disubstituted phenyl groups are sufficiently hindered to form only 1:1 complexes, as was originally shown by the isolation of $[Ni(pyN_2^{iPr2})L]$ species with L = $H_2O$ and $PMe_3$[51] and thereafter complex **1**.[19] Consequently, new members **2**−**5** of the hydroxo series **1**−**6** were prepared for kinetics study with $CO_2$.

Structures of hydroxo complexes **2**−**5**, set out in Figure 2, are planar; dimensions of **2** are typical.[29] Over the set **1**−**6**, the complexes are characterized by Ni−OH bond lengths in the interval 1.802(4)−1.835(9) Å and upfield hydroxyl proton shifts at $\delta$ −4.40 to −5.25. These signals are abolished by addition of small amount of $D_2O$. As seen in Figure 3, absorption spectra in DMF solutions show maxima near 410 nm and prominent shoulders at or near 450 nm. Given the utility of the main visible feature in monitoring reaction kinetics (see below), the origin of the UV/visible absorption bands was investigated by time-dependent DFT (TD-DFT). Computed spectra of **3** are shown in Figure 4, and additional details are found in Table 3. When the O−H group is constrained to the coordination plane, the principal band, a composite of two metal-to-ligand charge-transfer (MLCT) absorptions involving the pyridyl $\pi^*$ acceptor orbitals, occurs at 403 nm together with a second feature which is very weak compared to the experimental spectrum. When the O−H group is rotated out the plane by, for example, 60°, the principal band shifts to 370 nm and a prominent low-energy shoulder is generated at 425 nm. Hydroxo ligand rotation splits the MLCT transition between different 3d orbitals, resulting in a blue-shifted main absorption and a lower energy shoulder. Although the in-plane hydroxo conformation is calculated in the gas phase and observed in the solid state, solvent interactions may reorient the ligand in solution.

**Carbon Dioxide Fixation.** To compare the new fixation reactions reported here, it is useful to summarize previous results for complexes **1** and **7** and **6** and **12**.[19,25] (i) Absorption spectra of isolated $(Et_4N)[7]$ and the complex generated in solution by the minimal reaction $Ni^{II}{-}OH + CO_2 \rightarrow Ni^{II}{-}HCO_3$ are identical. (ii) The time dependence of UV/visible absorbance changes of the reaction system **1**/$CO_2$ in DMF at 400−450 nm fits accurately to a single exponential function indicating one resolvable process. (iii) The system **1**/$CO_2$ is second order with rate = $k_2'[\mathbf{1}][CO_2]$ and is described by the kinetics parameters in Table 4. (iv) Complex **6** with $CO_2$ forms **12**, which was isolated but reaction kinetics and the structure of **12** were not determined in previous work.

*(a). Reaction Systems.* Kinetics of the reactions of hydroxo complexes **2**−**6** with carbon dioxide in DMF (Figure 1) were investigated by stopped-flow techniques appropriate to processes that are complete in several seconds or less. Spectral changes are depicted in Figure 3 for the reactions of **2**−**5** and are similar to

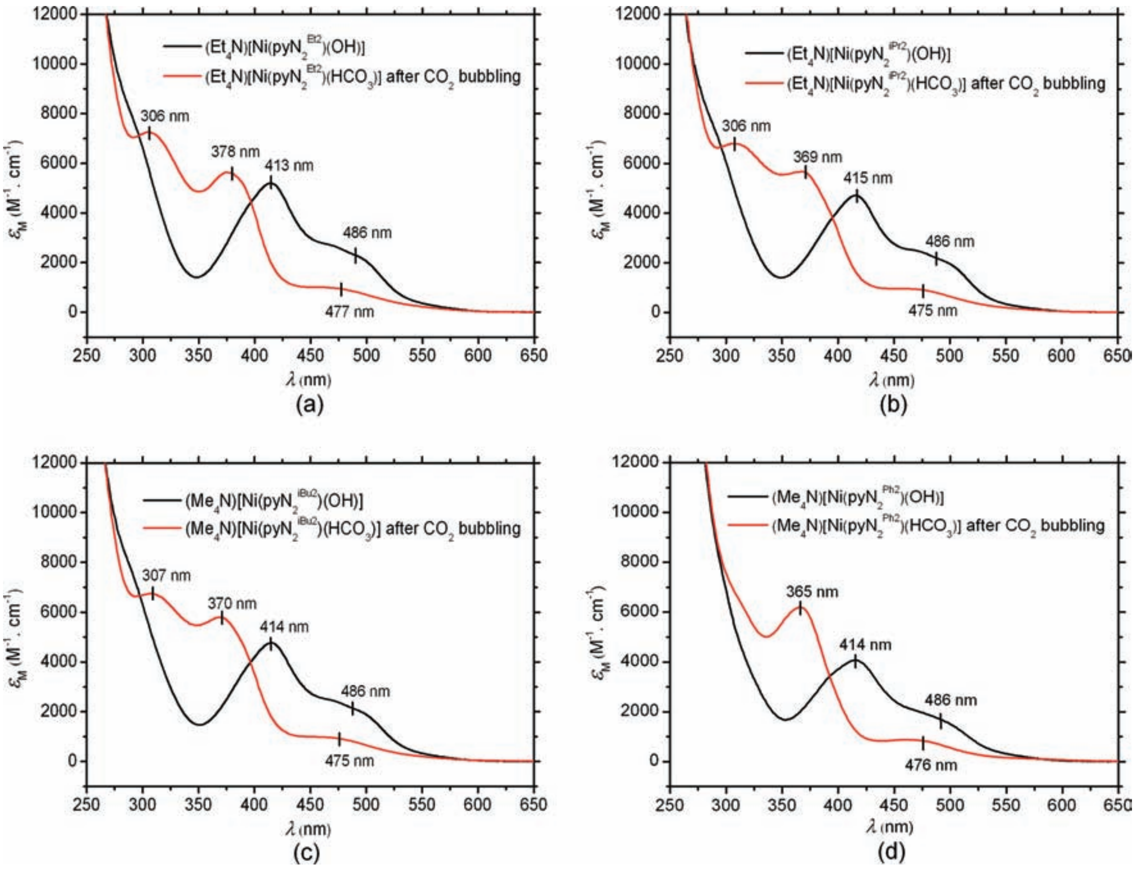

**Figure 3.** Absorption spectra of $[Ni^{II}(pyN_2^{R2})(OH)]^-$ and their reaction products after passing $CO_2$ through DMF solutions for 5−10 min. (a) R = Et, (b) R = $Pr^i$, (c) R = $Bu^i$, (d) R = Ph. Band maxima are indicated.

each other and to the reactions of **1** and **6**.[25] Spectra of typical complexes **2** and **8** are nearly identical in DMF and dichloromethane (Experimental Section), indicating that DMF is not acting as a ligand to hydroxo or bicarbonate complexes. Hereafter we designate the system with initial reactants **1** + $CO_2$ as the DMP system and that with **3** + $CO_2$ as the DIPP system. In all reaction systems, band intensities of the starting complexes near 415 nm and at 360−380 nm decrease and increase, respectively, as the bicarbonate reaction products **8**−**12** are formed. Products **8** and **9** (and **7** previously[25]) were isolated and identified by structure determinations. A preparative method is given for $(Et_4N)[$**8**$]$ (81% yield) but not for any compounds of **9**−**11** whose bicarbonate complexes proved too labile to loss of $CO_2$ to be isolated. Fortunately, a minute amount of crystalline $(Et_4N)[$**9**$]$ was isolated from DMF/ether after several weeks, allowing a structure determination. The structures of **8**, **9**, and **12** are included in Figure 2 and are shown from a side-on perspective in Figure 5 together with **7**. These views emphasize the $\eta^1$ binding mode of bicarbonate, the small deviations of the bound oxygen atoms from the $NiN_3$ plane, and the near or exact perpendicular orientations of this plane and the $CO_3$ plane. Among bicarbonate complexes, **7**, with the smallest ring substituents, is the most stable in DMF solution.

*(b). Kinetics.* Two types of kinetics behavior emerge. Absorbance data for the reactions of complexes **2**, **3**, and **4** displayed biphasic behavior indicative of two consecutive processes, and were fitted to a two-exponential equation. Taking the DIPP system as an example, absorbance changes at three wavelengths are shown in Figure 6. At the beginning, values at 385 and 421 nm increase and decrease, respectively, as formation of bicarbonate species begins (Figure 3). The data at 385 nm are the more revealing, showing a rapid growth in absorbance and subsequent slow decay. Similar observations were made for reactions of **2** and **4**. The fast process results in the formation of an intermediate from $[Ni(pyN_2^{R2})(OH)]^-$ and $CO_2$ and the slower process, which is independent of $CO_2$ concentration, affords the product bicarbonate complexes **8**−**10**. The time course of the reaction from reconstructed spectra of the DIPP system at 375−380 nm is provided in Figure 7. Initial complex **3** ($\lambda_{max}$ 415, 470−480 (sh) nm, spectrum **a**) forms an intermediate ($\lambda_{max}$ 375−385 nm, spectrum **b**) which converts to product **9** ($\lambda_{max}$ ~380, 450−460 (sh) nm, spectrum **c**). As shown in Figure 8, the fast process is dependent on $CO_2$ concentration whereas the slow process is not.

Noting that the ligand R-substituents are alkyl in the reactions of **2**, **3**, and **4**, we examined the similarly substituted DMP system at 380−390 nm in addition to 450 nm as previously. Rapid growth of absorbance was followed by slow and very small decay, suggesting that the intermediate and product spectra are very similar. Fits of the absorbance at 380 nm to a two-exponential rate law gave a pseudo-first-order rate constant $k_2$ identical to that evaluated from a one-exponential fit of the data at 450 nm.[19]

For phenyl-substituted complex **5** and macrocylic **6**, absorbance data at 370−500 nm and 223−243 K were best treated with single-exponential fits. For the reaction of **6**, data at three wavelengths show excellent fits to a single-exponential equation at 223 K in DMF, as seen in Figure 9. Note the absence of absorbance decay at 370 and 382 nm as the reaction proceeds. At 263 K and 370−390 nm, a rise and slight decay of absorbance was observed for **6**, suggesting an intermediate. However, spectral differences between intermediate and product in systems initially containing **5** and **6** are much less pronounced at this temperature than in reactions of **2**−**4**, such that kinetics parameters of a second step could not be reliably determined. The data for **6** in the lower temperature range demonstrate one fast, clean process of $CO_2$ binding uncomplicated by a subsequent slow process.

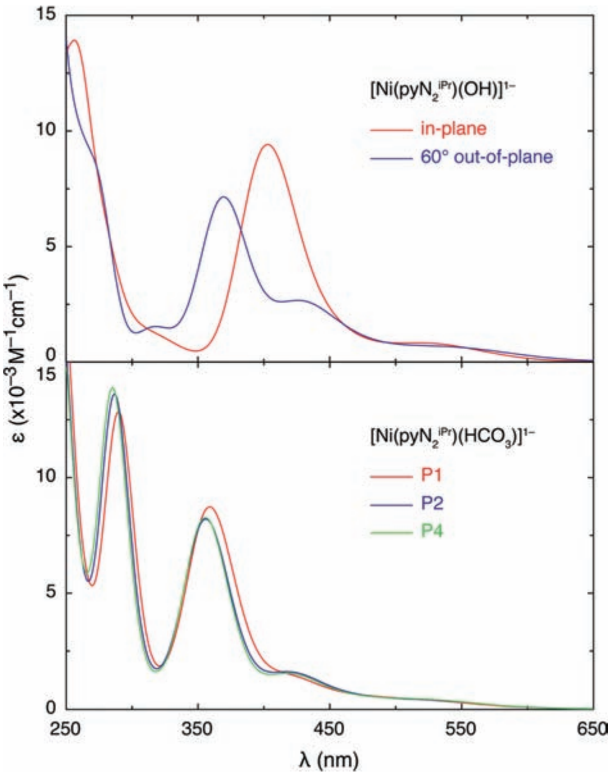

**Figure 4.** Absorption spectra (gas phase) computed by TD-DFT methodology. Upper panel: hydroxo complex **3** with Ni−O−H group in the coordination plane (red) or rotated by 60° out of the plane around the Ni−O bond (blue). Lower panel: bicarbonate complex **9** showing intermediate P1 (red) and conformers P2 (blue) and P4 (green).

The kinetics results demonstrate that all hydroxo complexes **1**−**6** react rapidly with $CO_2$ to form an intermediate which undergoes a much slower transformation to the product bicarbonate complexes **7**−**12**, completing the fixation reaction. Biphasic behavior is most clearly developed with **2**, **3**, and **4**, while **6** at low temperature is the most evident example of the fast process kinetically isolated from the slower process. If the slow process does occur, negligible spectral differences between the intermediate and bicarbonate product do not allow its spectrophotometric observation. Reactions were studied under pseudo-first-order conditions (large excess of $CO_2$). Exponential shapes of the kinetics traces of the fast reaction suggest that the reaction is first-order in $Ni^{II}$, and values of the rate constants do not depend on the initial $Ni^{II}$ concentration. Values of the observed rate constants increase with $CO_2$ concentration (Figure 8), establishing that the reaction is first order in $CO_2$. Consequently, for the fast process rate = $k_2'[Ni^{II}-OH][CO_2]$ where $k_2'$ is the second-order rate constant. The slow process is independent of $CO_2$ concentration and is described by rate = $k_1[Ni^{II}]$. An extensive

**Table 4. Kinetics Data for Carbon Dioxide Fixation by $[Ni(pyN_2{}^{R2}(OH)]^-$ Complexes and a Slow Subsequent Reaction in DMF Solutions**

| R | $\Delta H^‡$ (kcal/mol) | $\Delta S^‡$ (cal/(mol K))[a] | $k_2'{}^{233}$ ($M^{-1}$ $s^{-1}$) | $k_2'{}^{298}$ ($M^{-1}$ $s^{-1}$)[b] |
|---|---|---|---|---|
| | | Fast Process: $CO_2$ Fixation | | |
| Me[c] | 3.2 (5) | −20 | 1.75 (1) × $10^5$ | 9.5 × $10^5$ |
| Et | 2.0 (2) | −28 | 0.46 (2) × $10^5$ | 1.5 × $10^5$ |
| macro | 5.0 (1) | −17 | 1.90 (4) × $10^4$ | 2.7 × $10^5$ |
| $Pr^i$ | 3.0 (1) | −27 | 1.03 (2) × $10^4$ | 5.1 × $10^4$ |
| $Bu^i$ | 4.0 (1) | −25 | 3.40 (1) × $10^3$ | 2.8 × $10^4$ |
| Ph | 4.0 (2) | −27 | 1.17 (2) × $10^3$ | 9.5 × $10^3$ |

| R | $\Delta H^‡$ (kcal/mol) | $\Delta S^‡$ (cal/(mol K))[a] | $k_1{}^{233}$ ($s^{-1}$)[d] |
|---|---|---|---|
| | | Slow Process | |
| Et | 7.0 (1) | −27 | 1.4 (1) |
| $Pr^i$ | 10.0 (5) | −18 | 0.25 (1) |
| $Bu^i$ | 10.0 (1) | −19 | 0.118 (5) |

[a] Estimated standard deviation ±3 cal/(mol K). [b] Extrapolated value. [c] Ref 19. [d] Values independent of $[CO_2]$.

**Table 3. Computed Electronic Absorption Bands by TD-DFT in the DIPP Reaction System[a]**

| species | $\lambda_{max}$, nm ($\varepsilon_M$) | assignments |
|---|---|---|
| **3** (in-plane)[b] | 403 (9400) | Ni ($z^2$) → pyridyl ($\pi^*$) |
| | | Ni ($xz$) + carboxamide ($\pi$) → pyridyl ($\pi^*$) |
| **3** (60° out-of-plane)[b] | 370 (7100) | Ph ($\pi$) + carboxamide ($\pi$) → pyridyl ($\pi^*$) |
| | | Ni ($yz$) + OH (p)[d] → pyridyl ($\pi^*$) |
| | 425 (sh, 2700) | Ni (mixed d) + OH (p) → pyridyl ($\pi^*$) |
| | | Ni ($xz$) + carboxamide ($\pi$) → pyridyl ($\pi^*$) |
| P1[c] | 290 (12,800) | Ph ($\pi$) → Ni($x^2$-$y^2$) |
| | | carboxamide (O) → pyridyl ($\pi^*$) |
| | 359 (8700) | Ni ($yz$) → pyridyl ($\pi^*$) |
| | | Ph ($\pi$) + carboxamide ($\pi$) → pyridyl ($\pi^*$) |
| | 419 (sh, 1500) | Ni ($xz$) + carboxamide ($\pi$) → pyridyl ($\pi^*$) |

[a] B3LYP/6-31G(d), gas phase; coordinate system: $x$-axis along N−Ni−N, $y$-axis along $N_{py}$−Ni−O, $z$-axis perpendicular to coordination plane. [b] O−H group in coordination plane or rotated by 60° around the Ni−O bond out of the plane. [c] P2 and P4 (Figure 4) show nearly identical features to P1. P2: 287 (13,600), 356 (8200), 417 (sh, 1600) nm. P4: 285 (13,900), 355 (8300), 418 (sh, 1500) nm. [d] O p-orbital perpendicular to Ni−O−H plane.

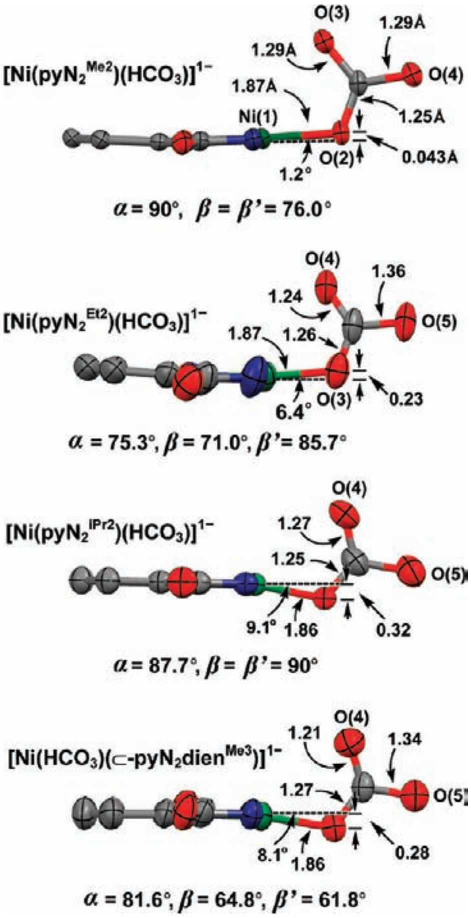

**Figure 5.** Structures of bicarbonate complexes **7**, **8**, **9**, and **12** viewed perpendicular to the chelate ring plane and showing the dihedral angles between planes: $\alpha$ = $NiN_3/CO_3$, $\beta$ and $\beta'$ = $NiN_3$/phenyl (two values). Also shown is the dihedral angle $NiN_3/NiN_2O$, the displacement (Å) of the coordinated oxygen atom from the $NiN_3$ plane, and the Ni−O and C−O distances (Å). The C−O(5) bond distance of **9** is not given because of disorder.

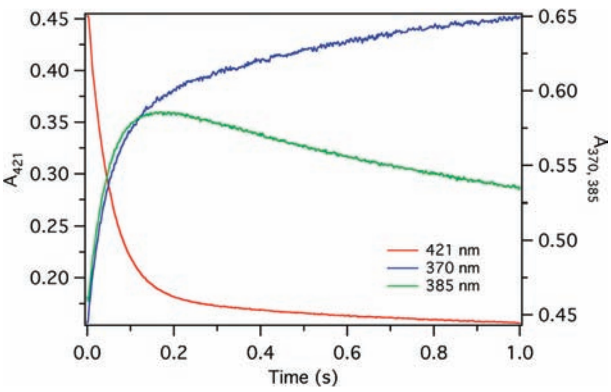

**Figure 6.** Kinetics traces at 370, 385, and 421 nm acquired for the DIPP system at 253 K in DMF: $[\mathbf{3}]_0$ = 0.1 mM, $[CO_2]_0$ = 1.0 mM.

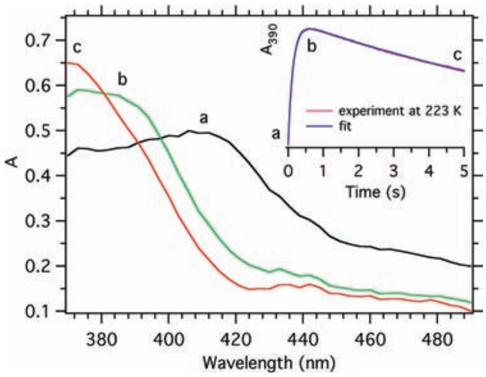

**Figure 7.** Spectra of **3** (a), intermediate in the reaction with $CO_2$ (b), and bicarbonate product **9** (c) reconstructed from single wavelength kinetics traces acquired at 253 K for the DIPP system in DMF: $[\mathbf{3}]_0$ = 0.1 mM, $[CO_2]_0$ = 1.0 mM. Inset: kinetics trace at 223 K and a fit of the data to a double-exponential rate law.

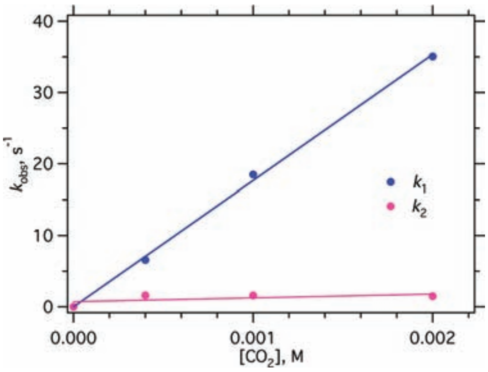

**Figure 8.** Plot showing dependence of rate constant on $[CO_2]$ for the fast process ($k_2$) and lack of dependence for the slow process ($k_1$). Data were acquired at 390 nm and 253 K in DMF with $[\mathbf{3}]_0$ = 0.1 mM and variable $[CO_2]$.

body of kinetics data on which the foregoing results are based is available.[29]

Reactions have been conducted under two other variable conditions that could bear on reaction mechanism.[29] Addition of 3200 equiv of $H_2O$ or $D_2O$ followed by kinetics measurements of the reaction between **3** and $CO_2$ in DMF at 223 K showed that $k_2'$ was reduced by about 50% compared to the system with no water added, consistent with a previous finding for **1** and $CO_2$.[19] Further, the ratio $k_2'$ $(D_2O)/k_2'$ $(H_2O)$ = 1.27, a result showing that breaking the O−H(D) bond is not involved in the rate-limiting step of $CO_2$ fixation with **3** and by implication with other members of the set **1**−**6**. Also, the presence or absence of water ($H_2O$ and $D_2O$) has no effect on the rate constant of the second process ($k_1$ = 0.09−0.11 $s^{-1}$). Variation of the concentration of **3** over the range 0.05−0.20 mM with excess $CO_2$ at 223 K yielded absorbance traces at 390 nm that were fit accurately with a double exponential rate law first-order in $Ni^{II}$ for both the fast and the slow processes. For the fast reaction, $k_2'$ = (9.5−8.9) × $10^3$ $M^{-1}$ $s^{-1}$, while for the slow reaction $k_1$ = 0.24−0.46 $s^{-1}$. Attempts to fit the latter reaction to a second-order rate law were unsatisfactory. The linear increase in $k_1$ with increasing $Ni^{II}$ concentration suggests a possible second-order $Ni^{II}$ contribution. However, a plot of the data reveals a large nonzero intercept corresponding to, primarily, a reaction first-order in $Ni^{II}$. These data do not clearly point to a process such as $\mu_2$-carbonate bridge formation as the origin of the slow reaction.

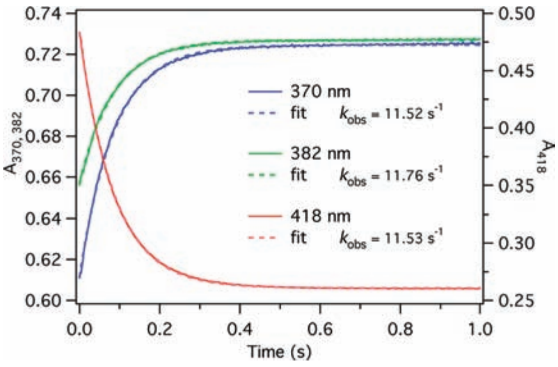

**Figure 9.** Kinetics traces at 370, 382, and 418 nm and their fits to a one-exponential rate law for the reaction between **6** and $CO_2$ in DMF at 223 K: $[\mathbf{6}]_0 = 0.1$ mM, $[CO_2] = 1.0$ mM. Rate constants are the averages of at least seven runs.

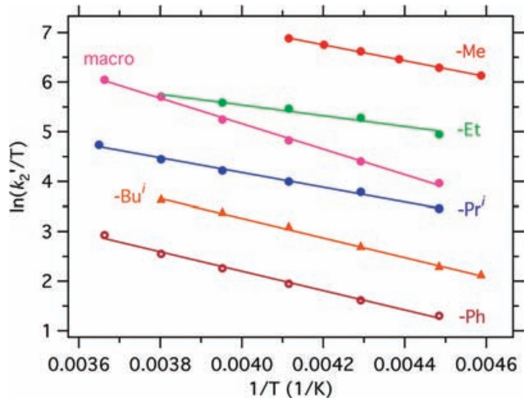

**Figure 10.** Eyring plots for the $CO_2$ fixation reactions of $[Ni^{II}(pyN_2^{R2})(OH)]^-$ and $[Ni(\subset\text{-}pyN_2dien^{Me3})(OH)]^-$ (macro) in DMF (Figure 1) as dependent on substituents R. $k_2' = k_{obs}/[CO_2]$; $[CO_2] = 1.0$ mM after mixing in the stopped flow instrument.

Temperature dependencies of rate constants for the fast processes of all reaction systems and slow processes in selected systems give excellent fits to the Eyring equation. Plots for the fast process are set out in Figure 10, and activation parameters are collected in Table 4 for the fast and slow processes. The negative activation entropies are consistent with a second order reaction and an associative transition state. At 233 K, $k_2'$ values follow order (3) written in terms of variable ligand substituents R. Numerical values are ratios of rate constants; for example, **5** reacts 123 times slower than **1**.

$$\mathrm{Me}(1) > \mathrm{Et}(3.2) > \mathrm{macro}(7.6) > \mathrm{Pr}^i(14) > \mathrm{Bu}^i(43) > \mathrm{Ph}(123) \qquad (3)$$

Eyring plots for systems with acyclic substituents are essentially parallel such that the rate order is unchanged over the temperature range. There is a qualitative trend toward slower rates as the steric size of the R groups increases. However, because of experimental uncertainties, this order does not correlate clearly with either $\Delta H^{\ddagger}$ or $\Delta S^{\ddagger}$ values. A rather typical trend in binding small molecules to metals is that increased activation entropies relate to less favorable binding because of limited access to the reactive site.[52] The macrocyclic reaction system differs from the others in that the Eyring plot is not parallel, and the position of macro and Et in series 3 must be inverted at 298 K. This system shows the lowest activation entropy, such that the contributions to $\Delta G^{\ddagger}$ from the activation entropy and enthalpy are practically equal.

*(c). Reaction Mechanism.* We have previously carried out a computational analysis of the energetics of the DMP system by DFT methods.[19] The DIPP system has been similarly analyzed in this work; the computed enthalpic reaction profile is given in Figure 11, and the energies and entropies of the equivalent stationary points in the two systems are compared in Table 5. The lowest energy pathway is summarized by the following sequence: (i) formation of a precursor complex (PC) by approach (ca. 2.5−3.0 Å) of the carbon atom of $CO_2$ to the hydroxo oxygen atom; (ii) insertion of $CO_2$ into the Ni−O bond to form a four-centered transition state ($TS_{ins}$); (iii) detachment of the Ni−OH bond to generate the Ni-$\eta^1$-$OCO_2H$ insertion product (P1); (iv) Ni−O bond rotations to the most stable bicarbonate conformers (P2 or P4 (not shown), in which the carbonyl oxygen atom and the hydroxyl proton are mutually *syn* or *anti*). The profiles for the two systems are quite similar; a detailed description of the DMP system is given elsewhere.[19]

For the DMP system, gas phase BP86/6-31G(d) calculations yield results that agree well with experimental findings in DMF solution. Overall, the computed energetics for the DIPP system differ little from those of the DMP system, with the calculated activation parameters for $CO_2$ insertion lower for the more hindered system by about 1.3 kcal/mol enthalpically and 3 cal/(mol K) entropically. Assuming that this step corresponds to the initial fast process observed experimentally, the changes in activation parameters agree with the kinetics measurements within acceptable errors for calculations of this type. On an absolute scale, the calculated activation enthalpy for the DIPP system is essentially identical with experiment, while the activation entropy deviates substantially in the negative direction. The same entropy error was observed in the DMP system and probably originates from the inaccurate description of low frequency vibrational modes.

Following the initial fast process of $CO_2$ insertion, what is the nature of the subsequent slow process found with the apparently more hindered ligand systems (**2**−**4**)? Given that the initial insertion product P1 is not predicted to be the most stable conformer, and P2 (or possibly P4 for the DIPP system) is the actual conformer observed crystallographically, it is tempting to ascribe the slow process to the rearrangement of the kinetic product P1 to the more stable bicarbonate orientations found in P2 and P4. The calculated barriers for these rearrangements relative to P1, however, differ little between the DIPP and DMP systems, and there is no slow process cleanly resolvable for the latter system. The $CO_2$ insertion is the rate-limiting step in our computational models for both systems. We have found no computational evidence for a subsequent high-barrier process in any of the reaction paths investigated. We also find a non-insertion pathway in which $CO_2$ forms an adduct Ni−O(H)$CO_2$ following by proton transfer to form a bicarbonate product to be substantially higher in energy (>10 kcal/mol) than the pathway of Figure 11.

Notwithstanding the predicted reaction energetics, the UV/visible spectra of the bicarbonate conformers in the DIPP system were calculated by TD-DFT to see if the intermediate P1 and products differ to any significant extent. As for hydroxo complex **3**, all primary bands of **9** are simulated by this approach using optimized geometries (Figure 4, Table 3). The theoretical maxima at 287, 356, and 417 (sh) nm of P2, for example, have

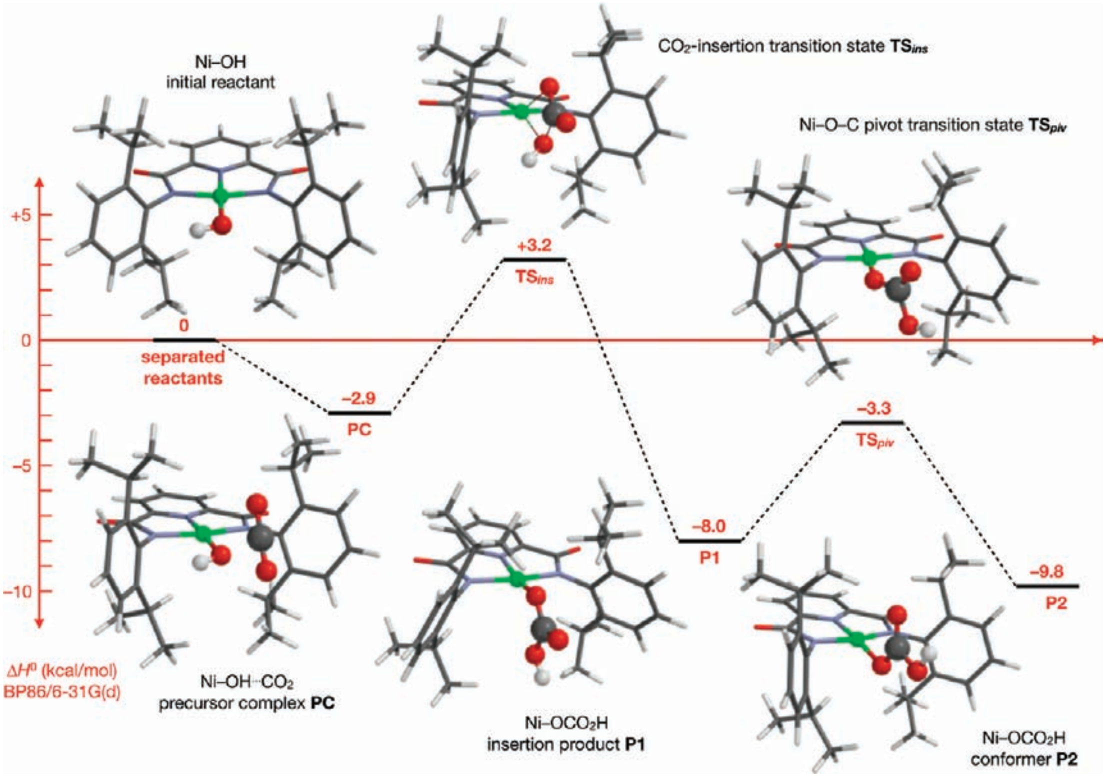

**Figure 11.** BP86/6-31G(d) reaction profile and stationary point structures for $CO_2$ fixation in the DIPP reaction system. Energy values (kcal/mol) are standard enthalpies of reaction or activation.

**Table 5. Computed Standard Reaction Enthalpies and Entropies (BP86/6-31G(d)) for the DMP and DIPP $CO_2$ Fixation Systems**[a]

| species[b] | DMP | DIPP |
|---|---|---|
| **PC** | −3.1[c] (−26)[d] | −2.9 (−26) |
| **$TS_{ins}$** | 4.5 (−36) | 3.2 (−39) |
| $TS_{pt}$ | 18.4 (−34) | 18.5 (−36) |
| **P1** | −7.9 (−34) | −8.0 (−35) |
| $TS_{piv12}$ | −2.2 (−38) | −3.3 (−40) |
| $TS_{rot12}$ | 1.3 (−40) | 1.3 (−41) |
| **P2** | −9.2 (−35) | −9.8 (−37) |
| $TS_{rot13}$ | −0.3 (−35) | −1.1 (−38) |
| P3 | −6.0 (−34) | −7.0 (−35) |
| $TS_{rot24}$ | −1.4 (−34) | −2.2 (−37) |
| P4 | −9.6 (−35) | −9.8 (−38) |
| $TS_{piv34}$ | −1.1 (−38) | −2.0 (−37) |
| $TS_{rot34}$ | −1.6 (−41) | −2.2 (−42) |

[a] Energies are referenced against the separated reactants using the conformer of **1** or **3** in which the phenyl rings of are canted toward each other on one side of the $NiN_3O$ coordination plane; this is the conformer observed crystallographically. An alternate conformation in which the rings are oriented roughly parallell to each other[19] is slightly lower in energy (−0.3 kcal/mol). [b] Bolded entries are defined in Figure 11; other entries refer to stationary points on the reaction pathway and are specified in ref 19 (Scheme 1). [c] Enthalpy, kcal/mol. [d] Entropy, cal/(mol K).

apparent experimental counterparts at 306, 369, and 475 nm. The two lower energy features contain MLCT components. While a close agreement cannot be expected between an experimental spectrum, particularly a reconstituted spectrum of non-optimal resolution, and a theoretical spectrum, we do associate spectrum **b** of the reaction intermediate in the DIPP system ($\lambda_{max}$ 375−380 nm, with a broad low-energy shoulder, Figure 7) with that of P1 ($\lambda_{max}$ 359, 419 (sh) nm). Spectrum **c** would then be related to the P2 and P4 spectra. The differences between the three computed spectra are so small that no structural differences can be inferred between the kinetic product of the fast process (P1) and the product of the slow process (P2 and/or P4). The nature of the latter remains to be determined.

**Summary.** The following are the principal results and conclusions of this investigation, including certain results from prior work.[19,25]

(1) Members of the family of planar complexes $[Ni^{II}(pyN_2^{R2})(OH)]^-$ containing tridentate 2,6-pyridinedicarboxamidate pincer ligands with variable 2,6-$C_6H_3R_2$ N-substituents and terminal hydroxo ligands are readily prepared.

(2) The complexes in (1) react cleanly and rapidly with $CO_2$ in DMF solution to afford the products $[Ni^{II}(pyN_2^{R2})(HCO_3)]^-$, some of which have been isolated. Bicarbonate complexes contain the $\eta^1$-$OCO_2H$ ligation mode with the $CO_3$ group nearly or exactly perpendicular to the coordination plane. These reactions are examples of $CO_2$ fixation.

(3) Fixation reactions are very rapid, low-barrier second-order processes with negative activation entropies indicative of associative transition states. At 298 K, rate constants $k_2'$ range from $9.5 \times 10^5$ (R = Me) to $9.5 \times 10^3$ $M^{-1}$ $s^{-1}$ (R = Ph), with the rate order overall correlating with the size of the R-substituent. Kinetics

comparisons with other metal-based $CO_2$ fixation systems are not highly accurate because these systems have been conducted in aqueous media.

(4) The majority of reaction systems are biphasic, showing a fast fixation reaction followed by a slow first order process ($k_1 \sim 0.1-1.4\ \mathrm{s}^{-1}$, 233 K) of currently unknown origin.

(5) Enthalpic reaction profiles for the R = Me and Pr$^i$ systems computed by DFT methods present a five-stage mechanism implicating a four-center (Ni-$\eta^2$-$OCO_2H$) transition state, an insertion product intermediate (Ni-$\eta^1$-$OCO_2H$), and bicarbonate reorientation to the stable product conformer. The insertion of $CO_2$ into a Ni−OH bond is a previously recognized event in the fixation process. In comparison, Co$^{\mathrm{III}}$ complexes react without bond-breaking,[1] as might be expected for six-coordinate low-spin reactants with lesser kinetic lability.

(6) Reaction rates are among the fastest reported for $CO_2$ fixation although comparisons are necessarily imprecise owing to solvent differences, with the large majority of existing data having been obtained in aqueous systems. However, the *intrinsic facility of the fixation reaction* is emphasized by the decrease in rate constant of only 100 at 298 K upon replacement of a small steric impediment (R = Me) near the reactive site with much larger groups (R = Bu$^i$, Ph).

Current research is directed toward an elucidation of the slow first-order process and of metal variation on the reaction rate.

## ■ ASSOCIATED CONTENT

**Ⓢ Supporting Information.** Crystallographic data for the compounds in Tables 1, 2 and the $Et_4N^+$ salt of [*N*,*N*′-bis(1-naphthyl)-2,6-pyridinedicarboximidato]Ni$^{\mathrm{II}}$, kinetics data pertinent to the reactions of [Ni$^{\mathrm{II}}$(pyN$_2^{\mathrm{R2}}$)(OH)]$^-$ with carbon dioxide. This material is available free of charge via the Internet at http://pubs.acs.org.

## ■ AUTHOR INFORMATION

### Corresponding Authors

*E-mail: sclee@uwaterloo.ca (S.C.L.), elena.rybak-akimova@tufts.edu (E.V.R.-A.), holm@chemistry.harvard.edu (R.H.H.).

## ■ ACKNOWLEDGMENT

This research was supported by grants from the National Science Foundation at Harvard University (CHE 084639) and at Tufts University (CHE 0750140 and CRIF CHE 0639138), and at the University of Waterloo by NSERC, CFI, ORF, and SHARCNET (computational facilities).

## ■ REFERENCES

(1) Palmer, D. A.; van Eldik, R. *Chem. Rev.* **1983**, *83*, 651–731.

(2) Acharya, A. N.; Dash, A. C. *Proc. Indian Acad. Sci. (Chem. Sci.)* **1993**, *105*, 225–233.

(3) Jacewicz, D.; Dabrowska, A.; Kolisz, I.; Chmurzynski, L.; Banecki, B.; Wozniak, M. *Transition Met. Chem.* **2005**, *30*, 209–216.

(4) Jacewicz, D.; Chylewska, A.; Daakbrowska, A.; Chmurzynski, L. *Z. Anorg. Allg. Chem.* **2007**, *633*, 1493–1499.

(5) Kitajima, N.; Hikuchi, S.; Tanaka, M.; Moro-oka, Y. *J. Am. Chem. Soc.* **1993**, *115*, 5496–5508.

(6) Kitajima, N.; Fujisawa, K.; Koda, T.; Hikuchi, S.; Moro-oka, Y. *J. Chem. Soc., Chem. Commun.* **1990**, 1357–1358.

(7) Murthy, N. N.; Karlin, K. D. *J. Chem. Soc., Chem. Commun.* **1993**, 1236–1238.

(8) Bazzicalupi, C.; Bencini, A.; Bencini, A.; Bianchi, A.; Corana, F.; Fusi, V.; Giorgi, C.; Paoli, P.; Paoletti, P.; Valtancoli, B.; Zanchini, C. *Inorg. Chem.* **1996**, *35*, 5540–5548.

(9) Looney, A.; Han, R.; McNeill, K.; Parkin, G. *J. Am. Chem. Soc.* **1993**, *115*, 4690–4697.

(10) (a) Zhang, X.; van Eldik, R. *Inorg. Chem.* **1995**, *34*, 5606–5614. (b) Nakata, K.; Shimomura, N.; Shiina, N.; Izumi, N.; Ichikawa, K.; Shiro, M. *J. Inorg. Biochem.* **2002**, 255–266. (c) Notni, J.; Schenk, S.; Görls, H.; Breitzke, H.; Anders, E. *Inorg. Chem.* **2008**, *47*, 1382–1390.

(11) Bergquist, C.; Fillebeen, T.; Morlok, M. M.; Parkin, G. *J. Am. Chem. Soc.* **2003**, *125*, 6189–6199.

(12) Peter, A.; Vahrenkamp, H. *Z. Anorg. Allg. Chem.* **2005**, *631*, 2347–2351.

(13) Zhang, X.; van Eldik, R.; Koike, T.; Kimura, E. *Inorg. Chem.* **1993**, *32*, 5749–5755.

(14) Company, A.; Jee, J.-E.; Ribas, X.; Lopez-Valbuena, J. M.; Gómez, L.; Corbella, M.; Llobet, A.; Mahia, J.; Benet-Buchholz, J.; Costas, M.; van Eldik, R. *Inorg. Chem.* **2007**, *46*, 9098–9110.

(15) Carmona, E.; Marín, J. M.; Palma, P.; Paneque, M.; Poveda, M. L. *Inorg. Chem.* **1989**, *28*, 1895–1900.

(16) Ito, M.; Takita, Y. *Chem. Lett.* **1996**, 929–930.

(17) Lozano, A. A.; Sáez, M.; Pérez, J.; García, L.; Lezama, L.; Rojo, T.; López, G.; García, G.; Santana, M. D. *Dalton Trans.* **2006**, 3906–3911.

(18) Wikstron, J. P.; Filatov, A. S.; Mikhalyova, E. A.; Shatruk, M.; Foxman, B. M.; Rybak-Akimova, E. V. *Dalton Trans.* **2010**, *39*, 2504–2514.

(19) Huang, D.; Makhlynets, O. V.; Tan, L. L.; Lee, S. C.; Rybak-Akimova, E. V.; Holm, R. H. *Proc. Natl. Acad. Sci. U.S.A.* **2011**, *108*, 1222–1227.

(20) Kieber-Emmons, M. T.; Schenker, R.; Yap, G. P. A.; Brunold, T. C.; Riordan, C. G. *Angew. Chem., Int. Ed.* **2004**, *43*, 6716–6718.

(21) Cámpora, J.; Palma, P.; del Rio, D.; Álvarez, E. *Organometallics* **2004**, *23*, 1652–1655.

(22) Cámpora, J.; Matas, I.; Palma, P.; Graiff, C.; Tiripicchio, A. *Organometallics* **2005**, *24*, 2827–2830.

(23) Adhikari, D.; Mossin, S.; Basuli, F.; Dible, B. R.; Chipara, M.; Fan, H.; Huffman, J. C.; Meyer, K.; Mindiola, D. J. *Inorg. Chem.* **2008**, *47*, 10479–10490.

(24) Powell-Jia, D.; Ziller, J. W.; DiPasquale, A. G.; Rheingold, A. L.; Borovik, A. S. *Dalton Trans.* **2009**, 2986–2992.

(25) Huang, D.; Holm, R. H. *J. Am. Chem. Soc.* **2010**, *132*, 4693–4701.

(26) Abbreviations are given in the Chart 1.

(27) Miura, Y.; Oka, H.; Momoki, M. *Synthesis* **1995**, 1419–1422.

(28) Sheldrick, G. M. *Acta Crystallogr.* **2008**, *A64*, 112–122.

(29) See paragraph at the end of this article for Supporting Information available.

(30) Gennaro, A.; Isse, A. A.; Vianello, E. *J. Electroanal. Chem.* **1990**, *289*, 203–215.

(31) Tezuka, M.; Iwasaki, M. *Chem. Lett.* **1993**, 427–430.

(32) Frisch, M. J. et al. *Gaussian 09*; Gaussian, Inc.: Wallingford, CT, 2009.

(33) Becke, A. D. *Phys. Rev. A* **1988**, *38*, 3098–3100.

(34) Perdew, J. P. *Phys. Rev. B* **1988**, *33*, 8822–8824.

(35) Rassolov, V. A.; Pople, J. A.; Ratner, M. A.; Windus, T. L. *J. Chem. Phys.* **1998**, *109*, 1223–1229.

(36) Rassolov, V. A.; Ratner, M. A.; Pople, J. A.; Redfern, J. A.; Curtiss, L. A. *J. Comput. Chem.* **2001**, *22*, 976–984.

(37) Stratmann, R. E.; Scuseria, G. E.; Frisch, M. J. *J. Chem. Phys.* **1998**, *109*, 8218–8224.

(38) Lee, C.; Yang, W.; Parr, R. G. *Phys. Rev. B* **1988**, *37*, 785–789.

(39) Miehlich, B.; Savin, A.; Stoll, H.; Preuss, H. *Chem. Phys. Lett.* **1989**, *157*, 200–206.

(40) Clark, T.; Chandrasekhar, J.; Spitznagel, G. W.; Schleyer, P. v. R. *J. Comput. Chem.* **1983**, *4*, 294–301.

(41) Dunning, T. H., Jr.; Hay, P. J. In *Modern Theoretical Chemistry*; Plenum: New York, 1976; pp 1−26.

(42) Tomasi, J.; Mennucci, B.; Cammi, R. *Chem. Rev.* **2005**, *105*, 2999–3093.

(43) O'Boyle, N. M.; Tenderholt, A. L.; Langner, K. M. *J. Comput. Chem.* **2008**, *29*, 839–845.

(44) Dennington, R.; Keith, T.; Millam, J. *GaussView*, Version 5; Semichem, Inc.: Shawnee Mission, KS, 2009.

(45) Mulliken, R. *J. Chem. Phys.* **1955**, *23*, 1833–1840.

(46) Tenderholt, A. L. *QMForge*, v. 2.1; Stanford University: Stanford, CA, 2007; http://qmforge.sourceforge.net.

(47) Patra, A. K.; Mukherjee, R. *Inorg. Chem.* **1999**, *38*, 1388–1393.

(48) Światek-Koslowska, J.; Gumienna--Kontecka, E.; Dobosz, A.; Golenya, I. A.; Fritsky, I. O. *Dalton Trans.* **2002**, 4639–4643.

(49) Alcock, N. W.; Clarkson, G.; Glover, P. B.; Lawrance, G. A.; Moore, P.; Napitupulu, M. *Dalton Trans.* **2005**, 518–527.

(50) Liu, S.-G.; Ni, C.-L. *Acta Crystallogr.* **2007**, *E63*, m1373–m1374.

(51) Wasilke, J.-C.; Wu, G.; Bu, X.; Kehr, G.; Erker, G. *Organometallics* **2005**, *24*, 4289–4297.

(52) Rybak-Akimova, E. V. In *Physical Inorganic Chemistry*; Bakac, A., Ed.; Wiley: New York, 2010; Vol. 2, pp 109−188.